Natural Hazards (2022) 111:641–660
https://doi.org/10.1007/s11069-021-05071-3

ORIGINAL PAPER

Amplification of soil moisture deficit and high temperature in a drought-heatwave co-occurrence in southwestern China

Lei Jiang[1,2] · Yongqin David Chen[3,4] · Jianfeng Li[1] · Cancan Liu[4]

Received: 21 January 2021 / Accepted: 1 October 2021 / Published online: 20 October 2021

Abstract

Co-occurrence events of droughts and heatwaves characterized by abnormal low soil moisture (SM) and high temperatures may cause more significant impacts on society and natural ecosystems than their individual occurrences. In addition to large-scale weather systems, regional land–atmosphere interactions significantly affect the development of co-occurrence events. In this study, weather research and forecasting model (WRF) was employed to evaluate the contributions of land–atmosphere interactions to a short-term drought-heatwave co-occurrence, which was the onset of the 2009/2010 extreme drought in southwestern China. The numerical experiments with perturbed SM show that the drought with SM deficit amplifies the heatwave severity, especially the afternoon's high temperature, by reducing latent cooling. The drought also tends to self-enhance through SM-precipitation feedback, as the simulated precipitation given lower SM is consistently less than the control run. The hotter/colder atmosphere experiments show that the heatwave also substantially affects the drought by altering land surface fluxes and atmospheric fields. Increases in latent heat in a hotter atmosphere reduce SM. Compared to the simulations for a colder atmosphere, simulated precipitation under a hotter atmosphere tends to be lower in a longer period before stronger precipitation occurs at the late stage of the concurrent event.

Keywords Drought · Heatwave · Drought-heatwave co-occurrence · Land–atmosphere interactions · Southwestern China

✉ Yongqin David Chen
ydavidchen@cuhk.edu.cn

✉ Jianfeng Li
jianfengli@hkbu.edu.hk

[1] Department of Geography, Hong Kong Baptist University, Hong Kong, China

[2] School of Marine Sciences, Nanjing University of Information Science and Technology, Nanjing, China

[3] School of Humanities and Social Science, The Chinese University of Hong Kong, Shenzhen, China

[4] Department of Geography and Resource Management, The Chinese University of Hong Kong, Hong Kong, China

1 Introduction

Global warming alters precipitation regimes as air temperature rises, resulting in more frequent and more intense droughts and heatwaves in recent decades, two of the most costly natural hazards to human society and the natural environment (Schar et al. 2004; Dai 2011; Li et al. 2018). For example, Europe has been significantly affected by summer heatwaves over the years, such as the 2003 heatwave causing heat-related mortality of around 35,000 people (Schar and Jendritzky 2004). Ding and Gao (2020) reported that a record-breaking extreme drought occurred in Yunnan Province in 2019, resulting in a significant reduction in agricultural production and direct economic losses of 6.562 billion yuan, higher than the total direct economic losses from the previous five years of drought. The summer heatwave over eastern China in 2013 affected more than half a billion people and caused enormous economic losses (Sun et al. 2014; Yuan et al. 2016).

The occurrence, evolution, and mechanism of droughts and heatwaves have been extensively investigated as separate events (e.g., Barriopedro et al. 2011; Dai 2011; Min et al. 2013; Russo et al. 2019). On the other hand, these two types of extreme events can be simultaneously triggered by the same large-scale abnormal weather systems such as persistent anticyclone systems, suggesting their origins can be physically correlated (Zeng et al. 2014; Tan et al. 2007). A co-occurrence of drought and heatwave can cause more significant impacts on society and the environment than their individual occurrences (IPCC 2013). Therefore, drought-heatwave co-occurrences have received increasing attention in recent years. The drought-heatwave co-occurrences have been found to increase significantly in China since the 1990s, and heat waves will coincide with most of the droughts in the 2010s (Ye et al. 2019). Zhang et al. (2019) found that concurrent droughts and heatwaves were projected to increase by 0.08–0.4 pentads per decade in 2006–2099 in China's Gan River Basin.

In addition to large-scale weather systems, regional land–atmosphere interactions are another essential mechanism in the development and propagation of droughts and heatwaves, especially the record-breaking events that occurred in different regions, such as in southwestern China (in 2009) (Ding and Gao 2020; Yang et al. 2012), and the United States (during 2013–2015) (Easterling et al. 2000; Fischer et al. 2007a,b). Soil moisture (SM) plays a crucial role in controlling heat balance between the land surface and atmosphere in the regional land–atmosphere interactions by partitioning of net radiation into latent (LH) and sensible heat fluxes (SH), which hence affects surface air temperature (Ferranti and Viterbo 2006; Fennessy and Kinter 2011; Chen et al. 2016). In a drought-heatwave co-occurrence, SM in deficit can be a crucial factor determining the partitioning, resulting in a significant reduction of latent cooling effect and raising surface air temperature (Seneviratne et al. 2010). Therefore, investigation on the sensitivity of surface air temperature changes to different SM levels is essential for understanding the impacts of regional land–atmosphere interactions on droughts and heatwaves. Zeng et al. (2011) conducted sensitivity experiments on land–atmosphere interactions by perturbing SM with a regional climate model to study SM's impacts on an extremely hot event in East China in 2003, and discovered the intensification of hot weather under low SM conditions. Furthermore, a negative correlation between spring soil moisture and the number of hot days in summer was found in North China, indicating that the soil moisture conditions have a significant effect on hot extremes (Wu and Zhang 2015).

Besides, how a heatwave may affect drought conditions is still not well understood and is debatable sometimes (Vicente-Serrano et al. 2014). Temperature increases tend

to raise evaporative demand, and soil may become drier if evaporation increases (Seneviratne et al. 2010; Zhang et al. 2018). Moreover, higher air temperature increases water vapor deficit and thus inhibits precipitation formation and increases drought severity (Wang et al. 2012). Diffenbaugh et al. (2015) found that warm conditions doubled the chances of drought years when precipitation deficiency occurred. On the other hand, some studies argued that high temperature is not the only driving factor of droughts through increases in water vapor demand because other meteorological variables (e.g., precipitation) and the exchange of heat and moisture of other regions may also change in a heatwave event (McVicar et al. 2012; Miralles et al. 2019; Sheffield et al. 2012). However, the research and understanding of these mechanisms are still limited so far. The responses of meteorological conditions and SM to the hot environment in a drought-heatwave co-occurrence event are the key to understand the different or even contradictory findings about the impacts of high temperature on droughts.

Previous studies mainly analyzed long-term climate simulations or observations to examine the impacts of high temperature on drought or how drought may enhance heatwave. However, the roles of land–atmosphere interactions may be different at various time scales (Zeng et al. 2014). Therefore, the importance of land surface processes on extreme weather simulations and predictions at short timescales has been highlighted in previous studies (e.g., Holt et al. 2006; Sun et al. 2012). A drought-heatwave co-occurrence event can last from days to weeks or as part of a long-lasting drought or heatwave event. A better understanding of the mechanisms of short-term concurrent events at fine temporal scales is crucial for enhancing our knowledge of the evolution of droughts/heatwaves and thus improving our weather forecast of high temperatures and dry conditions (Miralles et al. 2019; Zeng et al. 2014). Therefore, this study aims to examine the regional land–atmosphere interactions during a drought-heatwave co-occurrence event at high temporal and spatial resolutions using the Weather and Research Forecasting model (WRF).

The co-occurrence event we studied is the onset of a 100-year extreme drought in southwestern China in 2009/2010 (see Sect. 2). This severe drought event was associated with the lowest precipitation since 1880 and the most vital negative phase of Arctic Oscillation that impeded the moisture transport to southwestern China (Yang et al. 2012). Previous studies have reported that the 2009/2010 extreme drought was associated with evidently anomalous subsidence and strong negative-phase of Arctic Oscillation (Yang et al. 2012). However, how the regional land–atmosphere interactions affect the drought event is still unclear. The monthly SM simulations in southwestern China by the Variable Infiltration Capacity model from Li et al. (2016) show considerable negative monthly SM anomalies relative to the long-term monthly mean of 1961–2010 (Fig. 2). The lowest SM anomaly was observed in September 2009, indicating soil in that month is substantially drier than the long-term norm of September over the years. September 2009 was the onset of the extreme drought with a drop in monthly precipitation and a rise in air temperature (Zhang et al. 2012). SM and surface air temperature are perturbed in numerical experiments to evaluate the sensitivity of temperature to SM changes and SM's sensitivity to temperature changes in the co-occurrence event. The impact of the 2009/2010 drought-heatwave event in southwestern China is introduced in Sect. 2. The model setup and experimental design are described in Sect. 3. Section 4 first describes the comparison of our WRF simulations against *in situ* observations, and then presents the analysis of the experiment results and discussion of the physical mechanisms behind. Finally, a summary of findings and conclusions are given in Sect. 5.

2 Data and study area

2.1 Data

The 6-h National Centers for Environmental Prediction (NCEP) Final (FNL) Operational Global Analysis data at the 1° × 1° spatial resolution is obtained from https://rda.ucar.edu/datasets/ds083.2/. FNL is used as the meteorological initial and lateral boundary conditions for the WRF simulations. The FNL reanalysis data are from the Global Data Assimilation System of NCEP (Kalnay et al. 1996). Observed hourly 2-m air temperature (T2) data at Kunming, Luxi, and Zhanyi stations collected from the National Meteorological Information Center (NMIC) of China Meteorological Administration (CMA) are employed to validate the WRF simulations (Fig. 1).

2.2 Study area

The subtropical monsoon climate dominates southwestern China with wet summer and dry winter (Fig. 1). In this hilly area, about 900 mm annual precipitation is characterized by highly uneven spatial and temporal distributions (Liu et al. 2011). In recent years, a series of severe droughts have caused tremendous and extensive harmful impacts on agriculture production, food safety, water supplies, and natural ecosystems in southwestern China (Feng et al. 2014; Wang et al. 2014). In 2009–2010, southwestern China suffered from an extreme drought event with the severity of "once-in-a-century" and the lowest precipitation anomaly since 1880 (Yang et al. 2012; Zhang et al. 2012). The substantial destructive impacts of this extreme drought event have been reported in many previous studies (e.g., Qiu 2010; Liu et al. 2011). Agricultural production and drinking water supplies significantly dropped due to this drought event. Winter wheat productions in Yunnan and Guizhou provinces have been reported to reduce by 48% and 31%, respectively (Li et al. 2010; Zhang et al. 2012), and 18% of the population in Yunnan province (i.e., 8.1 million people) were short of drinking water (Qiu 2010). As the transitional zone between Qinghai-Tibet Plateau and China's southern plains, this area possesses unique ecosystems with high biodiversity where 44% of tree and vegetation species in the northern hemisphere can be found (Li 2000).

We further identify heatwaves in September 2009 based on the observed daily maximum T2 from the CMA. The heat wave is defined as a day with a temperature higher than a 90th percentile threshold of maximum temperature, and the threshold is calculated from the maximum temperature in a moving 5-day window centered on each calendar day of the base period (1961–1990) to account for the mean annual cycle in the study area (Chen et al. 2016; Klein Tank et al. 2009). Figure 2b shows a persistent heatwave event on 2–15 September 2009. Therefore, a co-occurrence event of drought and heatwave is detected in early September 2009, the onset of the 2009/2010 extreme drought. Based on numerical experiments by WRF, we analyze the interactions of SM and surface air temperature in this drought-heatwave event.

3 Model setup and experimental design

3.1 WRF model setup

WRF is a physically-based mesoscale numerical weather prediction model jointly developed by National Center for Atmospheric Research (NCAR), NOAA and other

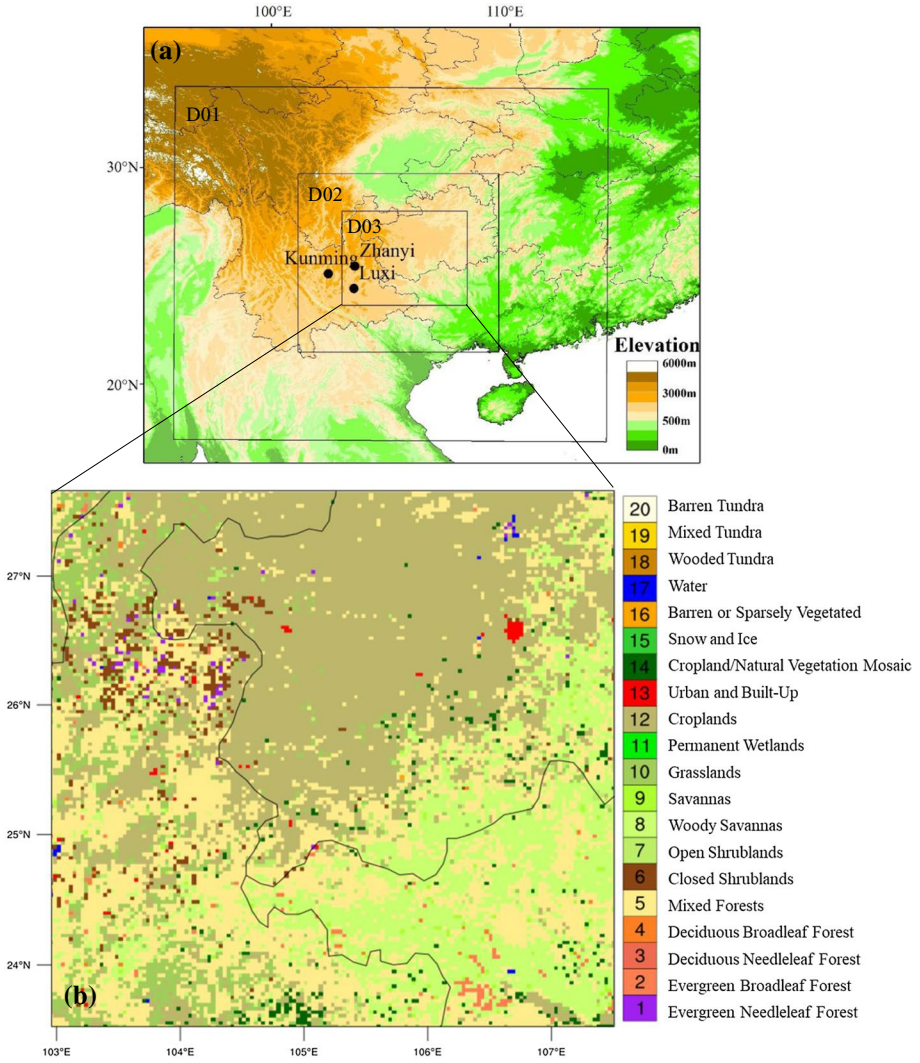

Fig. 1 **a** Location of southwest China and the domains in the WRF model setup. D01 is the outermost domain with 27 km grid resolution, D02 with 9 km resolution, and D03 the innermost domain with 3 km resolution. The solid squares denote the boundaries of the three domains, the black curves are the boundaries of Chinese provinces, and the black dots are the locations of meteorological stations used in this study. **b** Land use of D03

institutions for both research and forecasting purposes (Skamarock and Klemp 2008; Li et al. 2013). The model is capable of simulating the atmospheric circulation of the planetary boundary layer from the hemisphere to turbulence scales and has been widely used to conduct research investigations on various topics, such as urban heat islands (Lin et al. 2008; Chen et al. 2014), urban environmental problems (Chen et al. 2011), precipitation (Miao et al. 2009), and heatwaves (Zeng et al. 2011). WRF considers key

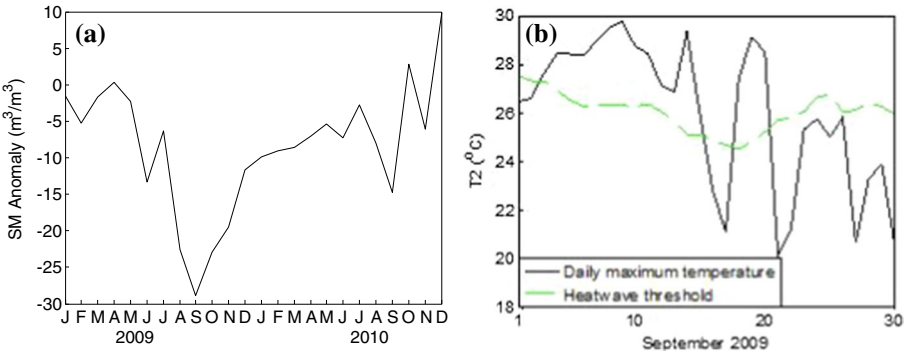

Fig. 2 **a** Anomalies of area-average monthly SM (m^3/m^3) in 2009 and 2010 relative to the long-term mean of the respective month during 1961–2010. **b** Area-average daily maximum T2 and the threshold of heatwave (i.e. the 90th percentile of 1971–2000) of the respective day in September 2009. A heatwave is detected if daily maximum T2 exceeds the threshold

features of atmospheric dynamics, such as fully compressible non-hydrostatic equations, Arakawa C grid, complete Coriolis, and curvature terms (Chen et al. 2011).

In this study, WRF 3.9.1 is configured with three two-way nested domains, i.e., D01, D02, and D03, in southwestern China with grid spacings of 27 km, 9 km, and 3 km, respectively (Fig. 1a). The largest domain D01 covers the southern part of China and the northern part of Southeast Asia; D02 covers the majority of southwestern China, including eastern Yunnan, southern Sichuan, Guizhou, and Guangxi provinces, and; the innermost domain D03 includes the core area of the analysis. The area coverage of D03 is consistent with the study regions in previous studies about the 2009/2010 extreme drought (e.g., Yang et al. 2012; Zhang et al. 2013). All simulations in WRF are from 00:00 on 1 September 2009 (local time) to 00:00 on 16 September 2009 (local time) with meteorological inputs from the NCEP FNL reanalysis dataset. It is necessary to spin up and let the model reach its own equilibrium after several hours of integration (Bonekamp et al. 2018; Jerez et al. 2020). In this study, 1 September 2009 is considered a spin-up period for model to reach its own equilibrium. Figure 1b shows the spatial distributions of land use for the D03 domain with croplands in the northern part and woody savannas in the south. The physical parameterization schemes adopted in this study include (1) the Single-Moment microphysics scheme (Lin et al. 1983), (2) the Betts–Miller–Janjic subgrid-scale cloud scheme (Janjic 1994), (3) the Rapid Radiation Transfer Model (RRTM) long-wave radiation scheme (Mlawer et al. 1997), (4) the Dudhia short-wave radiation scheme (Dudhia 1989), (5) the Monin–Obukhov surface layer scheme (Hong and Pan 1996), the Yonsei University (YSU) boundary layer parameterization scheme (Hong 2010), and (6) the Noah LSM scheme (Chen and Dudhia 2001; Ek et al. 2003). The details of the physical parameterization schemes are shown in Table 1.

3.2 Design of numerical experiments

We design two suites of numerical experiments to evaluate (1) the impacts of high air temperature on SM, and (2) the impacts of low SM on air temperature during the drought-heatwave co-occurrence event on 1–15 September 2009. For the first suite of experiments, following Zeng et al. (2014), air temperature of all vertical layers is modified

Table 1 Details of WRF model setup

Physical parameterization	D01	D02	D03
Number of horizontal grids	67*67	94*94	148*148
Spatial resolution (km)	27	9	3
Vertical layer	30	30	30
Simulation period (days)	15 days (00:00 1 September 2009–00:00 16 September 2009)		
Time step (s)	180	60	20
Microphysics	WRF Single-Moment 6-class (A scheme with ice, snow and graupel processes suitable for high-resolution simulations)		
Cumulus	Betts–Miller–Janjic		None
LW radiation	RRTM (Rapid Radiative Transfer Model)		
SW radiation	Dudhia shortwave radiation (Downward integration allowing efficiently for clouds and clear-sky absorption and scattering)		
PBL	MYJ PBL (One-dimensional prognostic turbulent kinetic energy scheme with local vertical mixing)		
LSM	Noah LSM (Unified NCEP/NCAR/AFWA scheme with soil temperature and moisture in four layers)		
Initial/boundary conditions	NCEP FNL analysis data (6-h interval, $1^\circ \times 1^\circ$ resolution)		

by + 1 °C (HOT1), + 2 °C (HOT2), + 3 °C (HOT3), + 4 °C (HOT4), + 5 °C (HOT5), − 1 °C (COLD1), − 2 °C (COLD2), − 3 °C (COLD3), − 4 °C (COLD4), and -5 °C (COLD5) in comparison with the CTL fields. The perturbance of air temperature is expected to alter the simulations of other land and atmospheric variables and fluxes, including humidity, precipitation, SH, LH, and SM. Simulations in the first suite of numerical experiments are conducted to evaluate SM's sensitivity to air temperature changes. Similarly, in the second suite of numerical experiments, the total volumetric SM content of each soil layer (i.e. 10, 30, 60 and 100 cm in the Noah LSM) at each grid is raised by 12.5% (hereafter WET12.5%), 25% (WET25%), 37.5% (WET37.5%), and 50% (WET50%), and reduced by 12.5% (DRY12.5%), 25% (DRY25%), 37.5% (DRY37.5%), and 50% (DRY50%) relative to the control condition (CTL). Other lateral boundary conditions are controlled. The simulations are then driven by the perturbed SM fields and other controlled lateral boundary conditions. Because the SM fields have been perturbed, other land and atmospheric variables as well as surface fluxes, such as air temperature, humidity, SH, and LH, over the simulation period also change. The simulation outputs of the first suite of experiments with various SM are compared to each other to analyze the impacts of SM changes on air temperature.

4 Results and discussion

4.1 Assessment of WRF model performance

We first assess the performance of WRF in southwestern China by comparing the CTL run with the in situ observations of hourly T2 in Kunming, Luxi, and Zhanyi (Fig. 3). The diurnal variations of simulated T2 fit the observations well at the three stations. WRF can capture the maximum T2 in the diurnal changes, although it tends to underestimate the minimum values. Because this study focuses on heatwave, the WRF performance in modeling high temperature is more critical. Furthermore, the correlation coefficients of the CTL run with the observations at the three stations are all above 0.9, and the linear regression coefficients are all close to 1, indicating the acceptable performance of WRF in simulating T2 in southwestern China.

4.2 Impacts of drought on the heatwave in the co-occurrence event

In the first suite of experiments (i.e., DRY50%, DRY37.5%, DRY25%, DRY12.5%, CTL, WET12.5%, WET25%, WET37.5%, and WET50%), SM fields are altered to different levels, and all other boundaries and initial conditions are controlled. Therefore, the comparison of the simulations of this suite of experiments shows the changes in T2 and other land and atmospheric variables due to the perturbed SM fields. The diurnal variations and spatial distributions of SM-induced changes in T2 are compared to each other to analyze SM wetting/drying impacts on T2.

T2 increases considerably when SM becomes lower in this drought-heatwave event (Fig. 4). The maximum increases of T2 are around 0.7 °C, 1.6 °C, 2.6 °C, and 3.8 °C in the DRY12.5%, DRY25%, DRY37.5%, and DRY50% experiments, respectively, which are mostly found in high temperatures in the afternoon. Meanwhile, nighttime T2 is less sensitive to the changes in SM. To better understand the sensitivity of daytime high T2 to SM changes, the sensitivity of T2 at 16:00 on 2 September 2009 to SM changes are shown in

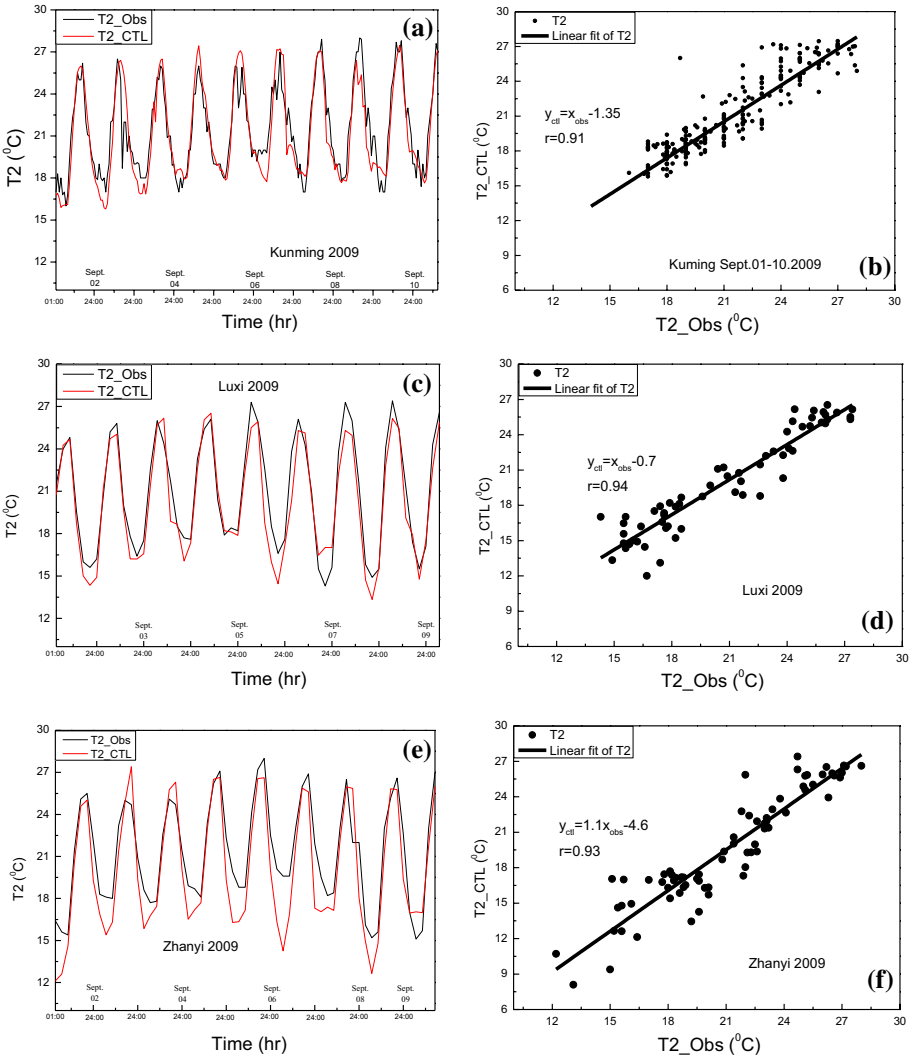

Fig. 3 Comparison of T2 of the CTL run against observations (Obs) in Kunming, Luxi, and Zhanyi on 1–10 September 2009. **a**, **c**, and **e** are the diurnal variations of T2. **b**, **d**, and **f** show the linear regressions and correlations between simulated and observed T2

Fig. 5. The time 16:00 is chosen because T2 generally reaches its daily maximum around this time, and the water vapor transmission and heat exchange between the land and atmosphere are the strongest within one day. T2 increases from about 24.5 °C to almost 28 °C if SM decreases from 100% in the CTL run to 50% in the DRY50% experiment.

Furthermore, the daily high T2 increases, and SM decreases show a nonlinear relationship. T2 tends to increase in a greater magnitude if the soil becomes further drier. Figure 6 shows the spatial distributions of T2 changes caused by the perturbed SM fields. In simulations with low SM, the largest increases in T2 are observed in the northeastern and eastern parts of the D03 domain. T2 increases by 3 °C in the majority of D03 in the DRY50%

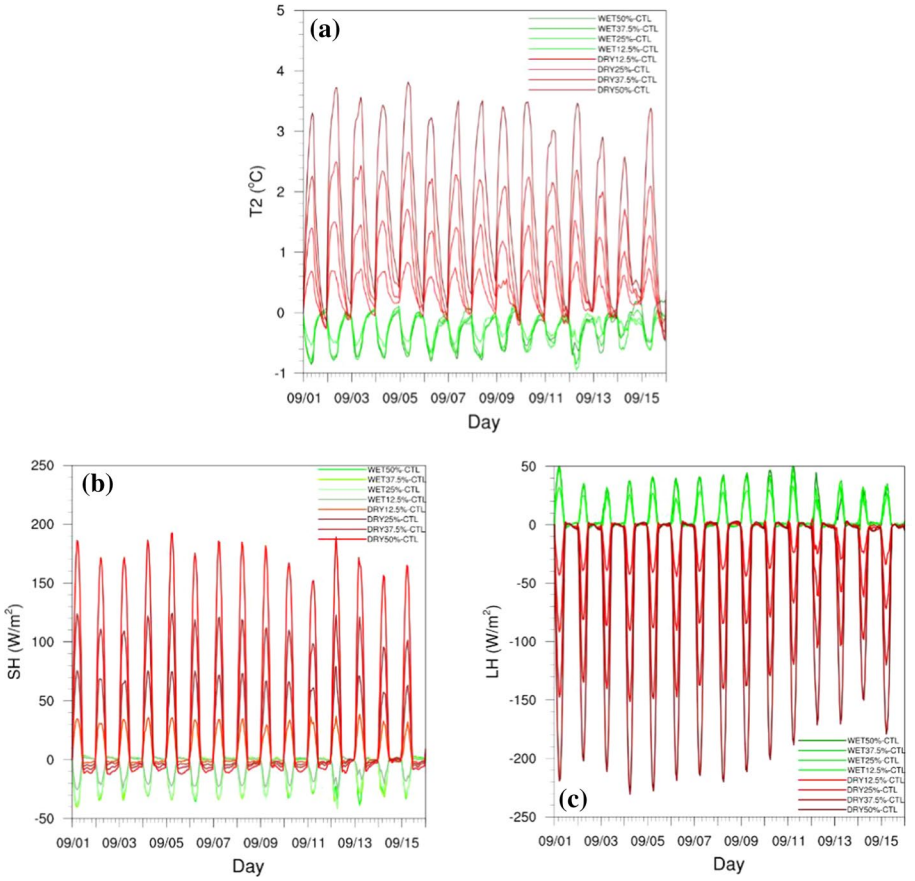

Fig. 4 Temporal evolutions of the differences of area-average **a** T2, **b** SH, and **c** LH of the simulations driven by perturbed SM fields relative to the CTL run over D03 in 2009

scenario. The spatial distribution of changes in T2 due to SM perturbation is highly correlated to topography and land use (Figs. 1 and 6). As the transition between the Qinghai-Tibet Plateau and China's southern plains, the terrain heights of the western parts of the D03 domain are higher than the eastern and southeastern parts. In the simulations with lower SM, the increases in T2 in the western parts are generally smaller than the eastern parts, e.g., T2 increases by about 1.5 °C in the western parts, but by 2–3 °C in the eastern parts in DRY50%. In other words, the magnitude of the increase in T2 in areas at higher altitudes in the west is smaller given the decreases in SM. In simulations with higher SM, the decreases in T2 are not as apparent as the increases in T2 in the DRY experiments (Figs. 4 and 6). When SM gets higher, T2 tends to be slightly lower than the CTL run, but the magnitude of changes is minimal. In the WET simulations, the afternoon's high temperatures decrease by less than 1 °C while the low temperatures at night change negligibly. The decreases in T2 due to SM increases are within -0.5 °C across southwestern China. Therefore, the results suggest that lower SM in this drought-heatwave event can amplify the heatwave severity, which is especially true for the daily high temperature in the afternoon. On the other hand, higher SM may slightly reduce the daily high temperature

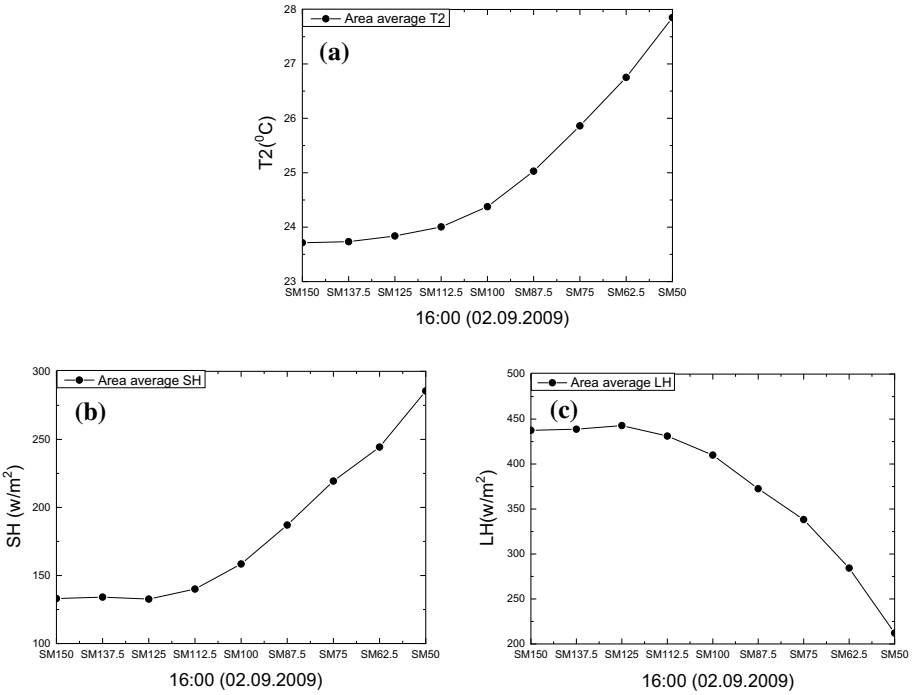

Fig. 5 The sensitivity of **a** T2, **b** SH, and **c** LH at 16:00 on 2 September 2009 to various SM values in D03. SM100 denotes the CTL run. SM150, SM137.5, …, SM50 denote the 150%, 137.5%, …, 50% SM relative to the CTL run in 2009

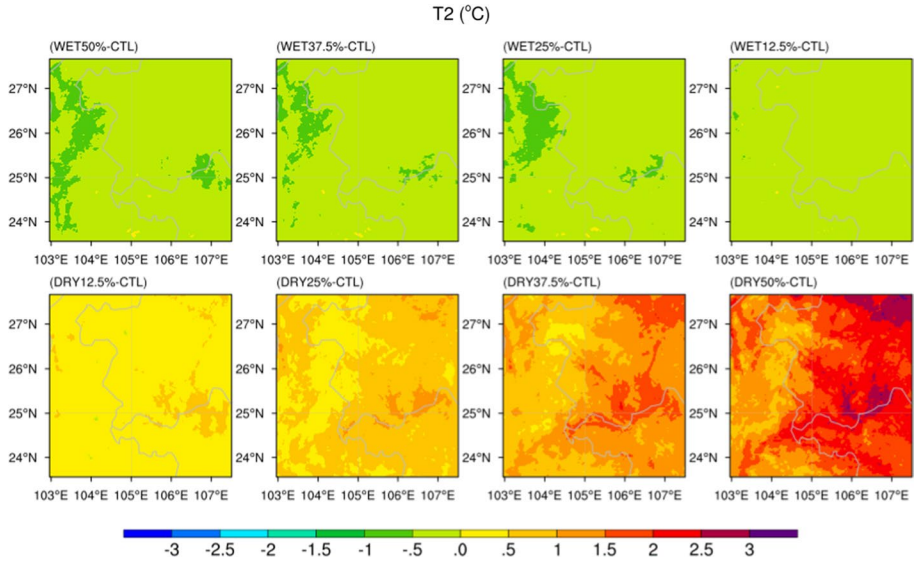

Fig. 6 Spatial distribution of the difference of the T2 between the perturbed SM experiments and the CTL run during 1–15 September 2009

and thus somewhat mitigate the heatwave. Generally, T2 increases more significantly in response to lower SM, but its reduction is less sensitive to higher SM.

4.3 Alterations in regional land–atmosphere interactions caused by SM deficiency

SM is the determining factor for partitioning the net radiation into SH and LH of the land surface. The upward SH from the land surface directly warms the low-level atmosphere and hence causes changes in T2. The changes in LH are determined by the changes in evaporation controlled by SM and air temperature. Therefore, an analysis of the changes of these regional land–atmosphere interactions associated with SM changes, especially SH and LH, can be used to explain the amplification of heatwave under SM drying.

When SM is lower, SH increases and vice versa (Fig. 4). SH changes to a greater extent under dry conditions than wet conditions in this event. Among the experiments, SH increases most substantially in the DRY50% case with increments of about 200 W/m^2 in the daytime. Similar to T2, SH at 16:00 on 2 September 2009 increases monotonically as SM decreases (Fig. 5). Figure 7 exhibits the spatial distribution of the SH differences between simulations driven by various SM fields compared to the CTL run. The largest increases in SH are around 60–80 W/m^2 in the western parts of D03 in the DRY50% simulation. Therefore, the increases in SH due to SM deficiency warms the low-level atmosphere as reflected by the T2 increases, leading to a more intense heatwave.

LH is the energy required for evaporation, which is determined by surface temperature, SM, and other factors (Liang et al. 1994). Drier soil causes a reduction in latent cooling (Fig. 4). In the DRY50% experiment, the largest reduction in LH is around 250 W/m^2. LH at 16:00 on 2 September 2009 decreases monotonically and nonlinearly as SM decreases from 125 to 50%, indicating that SM availability is the limiting factor of evaporation (Fig. 5). LH is found to be less sensitive to SM increases as LH remains

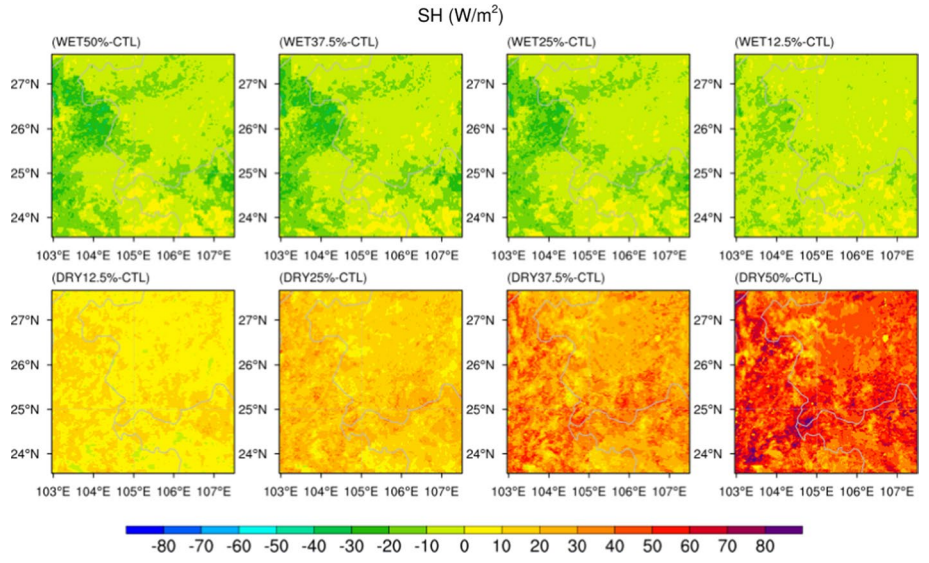

Fig. 7 Spatial distribution of the difference of the SH between the perturbed SM experiments and the CTL run during 1–15 September 2009

stable when SM increases from 125 to 150%, implying the available energy limits LH changes. The LH decreases due to SM deficiency are most significant in the western parts of D03, with decreases of about 70–80 W/m^2 in the DRY50% experiment (Fig. 8). SM is the determining factor for partitioning surface net radiation into SH and LH. Given the same net radiation, the LH decreases due to SM deficiency cause increases in SH, which warms the atmosphere and thus amplifies the heatwave. T2 is more sensitive to SM drying than SM wetting in this co-occurrence event. When SM increases from 100 to 150%, LH and SH are relatively stable, and hence T2 changes negligibly. Figure 4 also shows that T2, SH and LH at nighttime are insensitive to the SM changes. These results are observed because energy, instead of SM availability, is the controlling factor of evaporation under wet conditions and at nighttime (Roderick et al. 2009). This co-occurrence event is the onset of the 2009/2010 extreme drought. Therefore, SM is the limiting factor of evaporation under dry conditions, while energy availability plays such a role under wet conditions.

Furthermore, as shown in Fig. 9, the accumulative precipitation (AP) is lower with drier SM in this drought event through its impacts on evaporation and land surface fluxes. Accumulated precipitation is the sum of accumulated total cumulus precipitation in the study from the beginning of the simulations. Reductions of AP caused by SM deficiency suggest that the drought event can be self-amplified via the coupling of SM and precipitation (Seneviratne et al. 2010). The impacts of SM on evaporation play a vital role in the variations of SM-AP coupling, and the coupling is stronger in dry periods and dry regions (Wei and Drimeyer 2012). Therefore, the reductions in evaporation, as reflected by the LH decreases, due to SM deficiency, contribute to lower AP, further exacerbating the drought event.

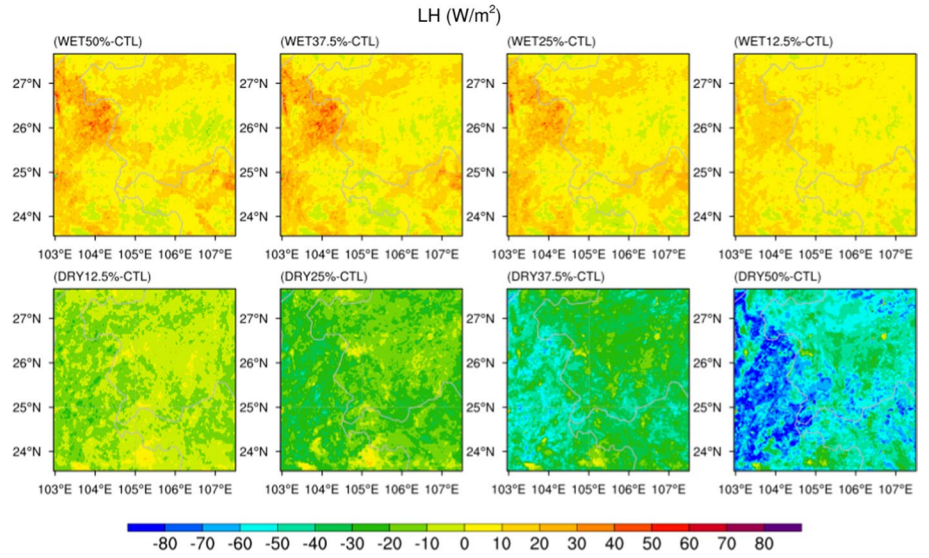

Fig. 8 Spatial distribution of the difference of the LH between the perturbed SM experiments and the CTL run during 1–15 September 2009

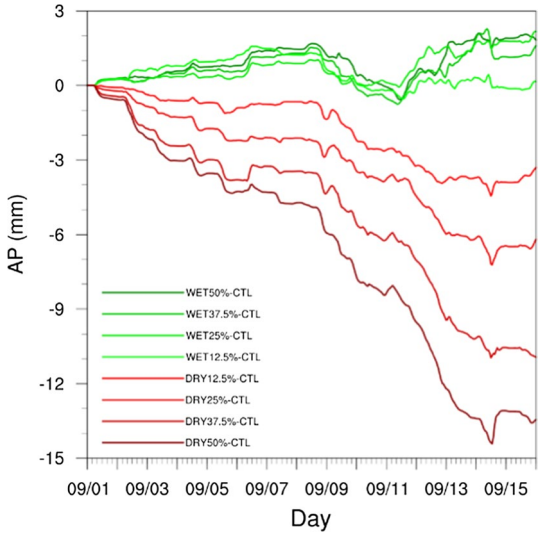

Fig. 9 Temporal evolution of area-average accumulative precipitation differences of simulations driven by the perturbed SM fields relative to the CTL run over the D03 domain

4.4 Impacts of the heatwave on drought severity and land surface fluxes

The SM of simulations driven by the modified atmospheric temperatures, i.e., HOT1, HOT2, HOT3, HOT4, HOT5, COLD1, COLD2, COLD3, COLD4 and COLD5, are compared to the CTL run to evaluate the sensitivity of SM to air temperature changes. In this suite of experiments, all vertical layers' air temperatures are modified, and other boundary conditions are the same in WRF. Therefore, the differences in the simulated SM are due to the modification of air temperatures.

The SM changes under various temperature perturbations demonstrate an inconsistent pattern as the drought event evolves (Fig. 10). Before 12 September, SM in the HOT experiments is lower than the CTL run, and SM in the COLD experiments is generally higher than the CTL run. SM in the HOT experiments increases substantially after 12 September, and the increase in HOT5 is more significant. Such increases in SM in the HOT experiments result from the precipitation input on 12 September, as shown by the AP increases on that day (Fig. 11). The AP differences between the experiments and CTL run suggest that the precipitation fields have been altered due to air temperature changes. Therefore, the SM changes in experiments with different temperature fields are considerably affected by precipitation changes. Before 5 September, AP in HOT experiments is larger than that in the COLD experiments (Fig. 11). In HOT experiments, more precipitation in a warmer atmosphere causes increases in SM around 2 September. However, SM decreases and becomes lower than the CTL run until the precipitation events on 12 September, implying the role of the changes in land surface fluxes in the hotter environment (Fig. 10). Understandably, SM decreases because evaporation increases as reflected by the LH increases in the HOT experiments. Because the AP of the HOT and COLD experiments are the closest during 1–5 September, the spatial distributions of SM during this period are compared to each other to minimize the impacts of differences in AP. The spatial distributions of the differences in SM relative to the CTL run are in line with that of LH during 1–5 September (Figs. 12 and 13). In the HOT experiments, SM decreases in D03 except in the western part, which agrees with LH increases in the same domain but reduces in the west part. If

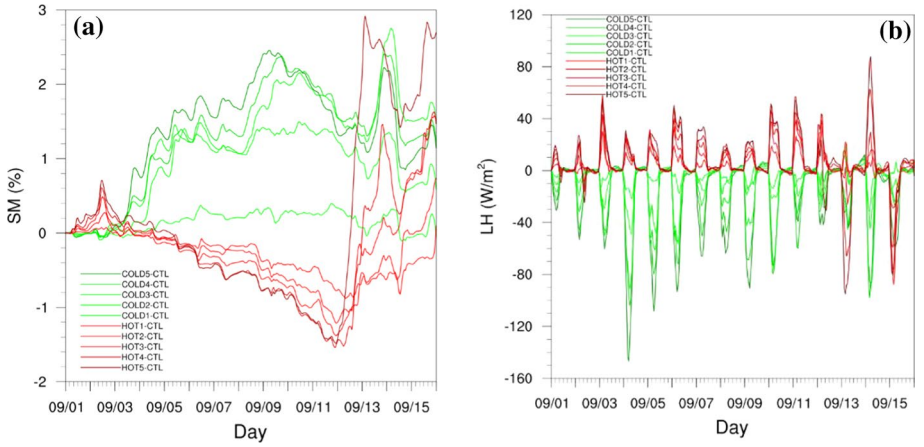

Fig. 10 Temporal evolutions of differences of area-average (a) SM and (b) LH of simulations driven by the perturbed air temperature fields relative to the CTL run over the D03 domain

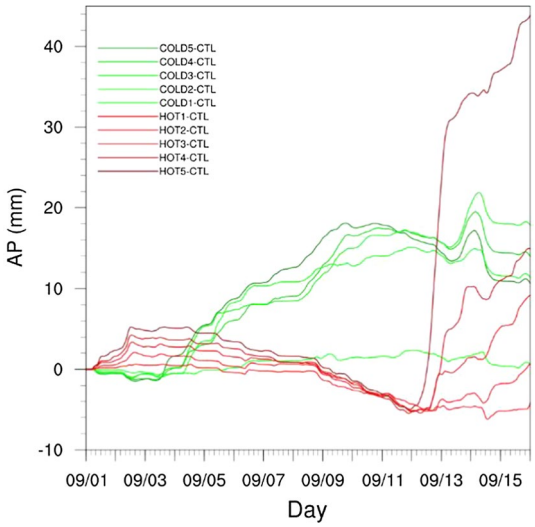

Fig. 11 Temporal evolution of the differences of area-average AP of simulations driven by the perturbed air temperature fields relative to the CTL run over the D03 domain

the temperature becomes lower, SM increases obviously due to the reduction in LH, especially in the northwestern part of D03.

The complexity of the responses of SM to temperature changes suggests that changes in air temperatures affect SM through alteration in precipitation and land surface fluxes. The temperature changes can alter other atmospheric variables, such as precipitation (Zeng et al. 2014). The temporal variations of SM from simulations of various perturbed temperature experiments are similar to AP's temporal changes (Figs. 10 and 11). Before the precipitation on 12 September, both AP and SM in the HOT experiments are generally less than the CTL runs, but higher in the COLD experiments. AP increases obviously in a short time due to the precipitation on 12 September. The difference of AP in HOT5 relative to the CTL run rises to 40 mm. The hotter atmosphere tends to produce less precipitation than the CTL run and the COLD experiments before 12 September. The precipitation event

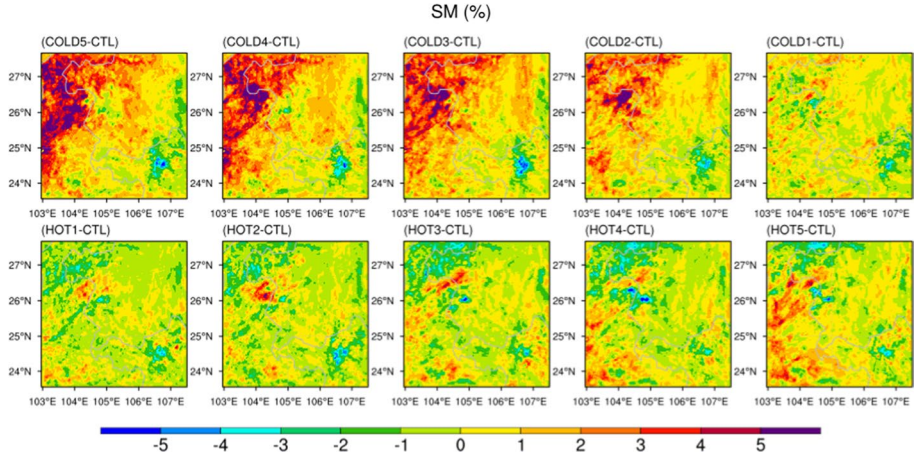

Fig. 12 Spatial distribution of the difference between the averages of SM during 1–5 September 2009 driven by the perturbed air temperatures and CTL fields

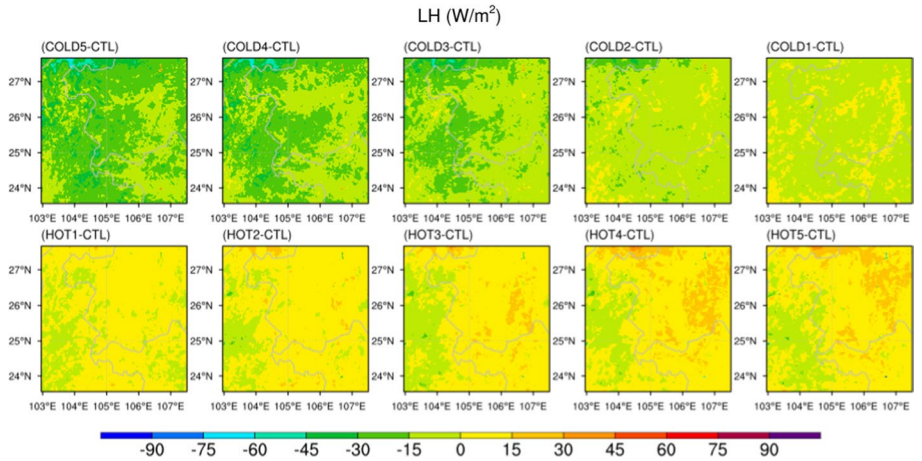

Fig. 13 Spatial distribution of the difference between the averages of LH during 1–5 September 2009 driven by the perturbed air temperatures and CTL fields

on that day is more intense in a hotter atmosphere. According to the Clausius–Clapeyron relation, the saturation water vapor content in the air is higher in a hotter atmosphere, thus reducing the chance of precipitation as relative humidity decreases, but possibly leading to more intense precipitation once it occurs because the hotter atmosphere has accumulated more water vapor (Lenderink et al. 2011). Therefore, in the HOT experiments, the dry duration tends to be longer, and precipitation is heavier once it occurs.

The changes in land surface fluxes due to higher air temperature are another primary mechanism for explaining SM's response to air temperature changes. The differences of AP of the HOT experiments with various temperature rise relative to CTL are similar around 11 September before the precipitation event (Fig. 11). Meanwhile, SM in experiments with larger temperature increases, e.g., HOT5, is lower than that in experiments with smaller temperature increases, e.g., HOT2, suggesting that the changes of regional land surface

fluxes reduce SM in a hotter environment. Higher air temperature enhances evaporation, as shown by the LH increases (Fig. 10).

In summary, air temperature changes can affect SM deficit via modification of atmospheric fields and regional surface fluxes. In this co-occurrence event of drought and heatwave, high air temperature alters precipitation fields, significantly affecting SM variations. At the same time, high temperature in the heatwave leads to more substantial evaporation and higher LH, further drying up the soil under drought condition.

5 Conclusions

In this paper, the interactions of SM and air temperatures in a drought-heatwave co-occurrence event during 1–15 September 2009 in southwestern China are evaluated by WRF coupled with Noah LSM. This co-occurrence event was the onset of the 2009/10 extreme drought in the region. The results of this modeling study help improve our understanding of the roles of regional land–atmosphere interactions in the emergence and development of drought-heatwave co-occurrence events. Two suites of numerical experiments with perturbed SM and air temperatures are conducted to analyze (1) the impact of SM deficit on T2, and (2) the sensitivity of SM to air temperature changes. The following conclusions can be drawn based on the study results:

1. SM deficit amplifies the heatwave severity in the co-occurrence event based on the experiments with perturbed SM. T2 increases by 1.5–3 °C in southwestern China, when SM reduces by 50% compared to the CTL run. The increases in T2 are most considerable in the afternoon when the air temperature reaches the daily maximum. In a drought event with low SM, SM is the limiting factor of evaporation, which is weaker in comparison with normal conditions, causing reductions in LH and hence increases in SH. The higher SH warms the low-level atmosphere, leading to increases in T2, i.e., amplification of heatwave in the drought-heatwave co-occurrence.
2. In this drought-heatwave co-occurrence, the drought with SM deficiency can be self-amplified through the coupling of SM and precipitation. SM and precipitation mutually interact and affect each other in a region. In the experiments with drier soil, precipitation decreases and is consistently lower than the CTL run over the study period. The reduction in precipitation makes the soil further drier, resulting in more intense drought conditions.
3. Further increases in temperature under the heatwave may amplify drought severity. Higher air temperature enhances evaporation as reflected by the LH increases, thus making the soil drier as the drought event progresses. Besides the changes in land surface fluxes, temperature increases also alter the precipitation fields, which also considerably affects the SM variations. Due to the increase in saturation water vapor content in a warmer atmosphere, a hotter atmosphere tends to elongate the dry duration.

Overall, in this co-occurrence event of drought and heatwave, SM deficit and high temperature significantly interact with and amplify each other through regional land–atmosphere interactions. Therefore, besides large-scale atmospheric dynamics, regional land–atmosphere interactions also play an essential role in the development and intensification of drought-heatwave co-occurrence events. Understanding this critical role

will provide scientific support to improve the forecasting and mitigation of drought and heatwave hazards.

Acknowledgements The work described in this paper was supported by the National Key R&D Program of China (2019YFC1510400), the National Natural Science Foundation of China (42071055), and the Research Grants Council of the Hong Kong Special Administrative Region, China (No. HKBU22301916 and No. HKBU12302518). The 6-hour NCEP FNL data are available at https://rda.ucar.edu/datasets/ds083.2/. Detailed information on the data can be obtained by contacting the corresponding authors at ydavidchen@cuhk.edu.cn or jianfengli@hkbu.edu.hk.

Data availability The data used in this study are available to the public in the websites provided in the manuscript. More details of the data can be obtained through writing to the corresponding authors.

Declarations

Conflict of interest The authors have no conflicts of interest.

References

Barriopedro D, Fischer EM, Luterbacher J, Trigo RM, Garcia-Herrera R (2011) The hot summer of 2010: redrawing the temperature record map of Europe. Science 332(6026):220–224

Bonekamp PNJ, Collier E, Immerzeel WW (2018) The impact of spatial resolution, land use, and spinup time on resolving spatial precipitation patterns in the Himalayas. J Hydrometeorol 19(10):1565–1581. https://doi.org/10.1175/JHM-D-17-0212.1

Chen F, Dudhia J (2001) Coupling an advanced land-surface hydrology model with the Penn State-NCAR MM5 modeling system. Part 1: model description and implementation. Mon Weather Rev 129:569–585

Chen F, Kusaka H, Bornstein R, Ching J, Grimmond C, Grossman-Clarke S, Loridan T, Manning KW, Martilli A, Miao S (2011) The integrated WRF/urban modelling system: development, evaluation, and applications to urban environmental problems. Int J Climatol 31:273–288

Chen F, Yang X, Zhu W (2014) WRF simulations of urban heat island under hot-weather synoptic conditions: the case study of Hangzhou City, China. Atmos Res 138:364–377

Chen YD, Li J, Zhang Q (2016) Changes in site-scale temperature extremes over China during 2071–2100 in CMIP5 simulations. J Geophys Res Atmos. https://doi.org/10.1002/2015JD024287

Dai A (2011) Drought under global warming: a review. WIRES Clim Change 2:45–65

Diffenbaugh NS, Swain DL, Touma D (2015) Anthropogenic warming has increased drought risk in California. PNAS 112(13):3931–3936

Ding T, Gao H (2020) The record-breaking extreme drought in Yunnan province, Southwest China during spring-early summer of 2019 and possible causes. J Meteorol Res 34(5):997–1012

Dudhia J (1989) Numerical study of convection observed during the winter monsoon experiment using a meso scale two-dimensional model. J Atmos Sci 46:3077–3107

Easterling DR, Meehl GA, Parmesan C, Changnon SA, Karl TR, Mearns LO (2000) Climate extremes: observations, modeling, and impacts. Science 289(5487):2068–2074

Ek MB, Mitchell KE, Lin Y, Rogers E, Grunmann P, Koren V, Gayno G, Tarpley JD (2003) Implementation of Noah land surface model advances in the National Centers for Environmental Prediction operational mesoscale Eta model. J Geophys Res 108(D22):8851. https://doi.org/10.1029/2002JD003296

Feng L, Li T, Yu W (2014) Cause of severe droughts in Southwest China during 1951–2010. Clim Dyn 43(7–8):2033–2042

Fennessy MJ, Kinter JL III (2011) Climatic feedbacks during the 2003 European heat wave. J Clim 24:5953–5967

Ferranti L, Viterbo P (2006) The European summer of 2003: Sensitivity to soil water initial conditions. J Clim 19:3659–3680

Fischer EM, Seneviratne SI, Luthi D, Schar C (2007a) Contribution of land-atmosphere coupling to recent European summer heat waves. Geophys Res Lett 34:L06707. https://doi.org/10.1029/2006GL029068

Fischer EM, Seneviratne SI, Lüthi D, Schär C (2007b) Soil Moisture–atmosphere interactions during the 2003 European summer heat wave. J Clim 20:5081–5099

Holt T, Niyogi D, Chen F, LeMone MA, Manning K, Qureshi AL (2006) Effect of land-atmosphere interactions on the IHOP 24–25 May 2002 convection case. Mon Weather Rev 134:113–133
Hong S-Y (2010) A new stable boundary-layer mixing scheme and its impact on the simulated East Asian summer monsoon. Q J R Meteorol Soc 136:1481–1496
Hong S-Y, Pan H-L (1996) Nonlocal boundary layer vertical diffusion in a medium-range forecast model. Mon Weather Rev 124:2322–2339
IPCC (2013) Climate change 2013: the physical science basis. Contribution of working group I to the fifth assessment report of the intergovernmental panel on climate change. Cambridge University Press, Cambridge
Janjic ZI (1994) The step-mountain eta coordinate model: further developments of the convection, viscous sublayer, and turbulence closure schemes. Mon Weather Rev 122:927–945
Jerez S, Lopez-Romero JM, Turco M, Lorente-Plazas R, Gomez-Navaro JJ, Jimenez-Guerrero P, Montavez JP (2020) On the spin-up period in WRF simulations over Europe: trade-offs between length and seasonality. J Adv Model Earth Syst. https://doi.org/10.1029/2019MS001945
Kalnay E, Kanamitsu M, Kistler R et al (1996) The NCEP/NCAR 40-year reanalysis project. Bull Am Meteorol Soc 77(3):437–471
Klein Tank AMG, Zwiers FW, Zhang X (2009) Guidelines on analysis of extremes in a changing climate in support of informed decisions for adaptation. WCDMP-72. World Meteorological Organization, Geneva, Switzerland
Lenderink G, Mok HY, Lee TC, van Oldenborgh GJ (2011) Scaling and trends of hourly precipitation extremes in two different climate zones—Hong Kong and the Netherlands. Hydrol Earth Syst Sci 15:3033–3041
Li W (2000) Problems of ecological environment conservation in Southwest China. Sci Silvae Sin 36(5):10–11
Li Q, Yan N, Zhang F, Wu B (2010) Drought monitoring and its impacts assessment in Southwest China using remote sensing in the spring of 2010. Acta Geophys Sin 65:771–780 (**in Chinese**)
Li D, Bou-Zeid E, Barlage M, Chen F, Smith JA (2013) Development and evaluation of a mosaic approach in the WRF-Noah framework. J Geophys Res Atmos 118:11918–11935
Li J, Zhang L, Shi X, Chen YD (2016) Response of long-term water availability to more extreme climate in the Pearl River Basin. China. Int J Climatol 37(7):3223–3237
Li J, Chen YD, Gan TY, Lau N-G (2018) Elevated increases in human-perceived temperature under climate warming. Nat Clim Chang 8:43–47. https://doi.org/10.1038/s41558-017-0036-2
Liang X, Lettenmaier DP, Wood EF, Burges SJ (1994) A simple hydrologically based model of land surface water and energy fluxes for general circulation models. J Geophys Res Atmos 99(D7):14415–14428
Lin Y-L, Farley RD, Orville HD (1983) Bulk parameterization of the snow field in a cloud model. J Clim Appl Meteorol 22:1065–1092
Lin C-Y, Chen F, Huang JC, Chen W-C, Liou Y-A, Chen W-N, Liu S-C (2008) Urban heat island effect and its impact on boundary layer development and land-sea circulation over northern Taiwan. Atmos Environ 42:5635–5649
Liu J, Tan X, Wan J, Ma J, Zhang N (2011) Comparative analysis between 2010 severe drought in Southwest China and typical drought disasters. China Water Resour 9:17–20 (**in Chinese**)
McVicar TR et al (2012) Global review and synthesis of trends in observed terrestrial near-surface wind speeds: implications for evaporation. J Hydrol 416(417):182–205
Miao S, Chen F, LeMone MA, Tewari M, Li Q, Wang Y (2009) An observational and modeling study of characteristics of urban heat island and boundary layer structures in Beijing. J Appl Meteorol Climatol 48:484–501
Min E, Hazeleger W, Oldenborgh GJ, Sterl A (2013) Evaluation of trends in high temperature extremes in north-western Europe in regional climate models. Environ Res Lett 8:014011
Miralles DG, Gentine P, Seneviratne SI, Teuling AJ (2019) Land-atmospheric feedbacks during droughts and heatwaves: state of the science and current challenges. Ann N Y Acad Sci 1436(1):19–35. https://doi.org/10.1111/nyas.13912
Mlawer EJ, Taubman SJ, Brown PD, Iacono MJ, Clough SA (1997) Radiative transfer for inhomogeneous atmospheres: RRTM, a validated correlated-k model for the longwave. J Geophys Res 12(D14):16663–16682
Qiu J (2010) China drought highlights future climate threats. Nature 465:142–143
Roderick ML, Hobbins MT, Farquhar GD (2009) Pan evaporation trends and the terrestrial water balance. II. Energy balance and interpretation. Geogr Compass 3(2):761–780
Russo S, Sillmann J, Sippel S, Barcikowska MJ, Ghisetti C, Smid M, O'Neil B (2019) Half a degree and rapid socioeconomic development matter for heatwave risk. Nat Commun 10:136
Schar C, Jendritzky G (2004) Hot news from summer 2003. Nature 432:559–560

Schar C, Vidale PL, Luthi D, Frei C, Haberli C, Liniger MA, Appenzeller C (2004) The role of increasing temperature variability in European summer heatwaves. Nature 427(322):332–336
Seneviratne SI, Corti T, Davin EL et al (2010) Investigating soil moisture-climate interactions in a changing climate: a review. Earth Sci Rev 99:125–161
Sheffield J, Wood EF, Roderick ML (2012) Little change in global drought over the past 60 years. Nature 491:435–438
Skamarock WC, Klemp JB (2008) A time-split nonhydrostatic atmospheric model for weather research and forecasting applications. J Comput Phys 227:3465–3485
Sun J, Trier SB, Xiao Q, Weisman ML, Wang H, Ying Z, Xu M, Zhang Y (2012) Sensitivity of 0–12 h warm-season precipitation forecasts over the central United States to model initialization. Weather Forecast 27:832–855
Sun Y, Zhang X, Zwiers FW, Song L, Wan H, Hu T, Yin H, Ren G (2014) Rapid increase in the risk of extreme summer heat in Eastern China. Nat Clim Change 4:1082–1085
Tan J, Zheng Y, Song G (2007) Heat wave impacts on mortality in Shanghai, 1998 and 2003. Int J Biometeorol 51:193–200
Vicente-Serrano SM, Lopez-Moreno J-I, Begueria S et al (2014) Evidence of increasing drought severity caused by temperature rise in southern Europe. Environ Res Lett 9:044001
Wang K, Dickinson RE, Liang S (2012) Global atmospheric evaporative demand dover land from 1973 to 2008. J Clim 25:8353–8361
Wang L, Chen W, Zhou W (2014) Assessment of future drought in Southwest China based on CMIP5 multi-model projections. Adv Atmos Sci 31:1035–1050
Wei J, Dirmeyer PA (2012) Dissecting soil moisture-precipitation coupling. Geophys Res Lett 39(19):L19711. https://doi.org/10.1029/2012GL053038
Wu L, Zhang J (2015) The relationship between spring soil moisture and summer hot extremes over North China. Adv Atmos Sci 32(12):1660–1668
Yang J, Gong D, Wang W, Hu M, Mao R (2012) Extreme drought event of 2009/2010 over Southwestern China. Meteorol Atmos Phys 115:173–184
Ye L, Shi K, Xin Z, Wang C, Zhang C (2019) Compound droughts and heat waves in China. Sustainability 11(12):3270
Yuan W, Cai W, Chen Y et al (2016) Severe summer heatwave and drought strongly reduced carbon uptake in Southern China. Sci Rep 6:18813
Zeng X-M, Wu Z-H, Xiong S-Y, Song S, Zheng Y-Q, Liu H-Q (2011) Sensitivity of simulated short-range high-temperature weather to land surface schemes by WRF. Sci China Earth Sci 54:581–590
Zeng X-M, Wang B, Zhang Y, Song S, Huang X, Zheng Y, Chen C, Wang G (2014) Sensitivity of high-temperature weather to initial soil moisture: a case study using the WRF model. Atmos Chem Phys 14:9623–9639
Zhang L, Xiao J, Li J, Wang K, Lei L, Guo H (2012) The 2010 spring drought reduced primary productivity in Southwestern China. Environ Res Lett 7:045706
Zhang W, Jin F-F, Zhao J-X, Qi L, Ren H-L (2013) The possible influence of a nonconventional El Nino on the severe autumn drought of 2009 in Southwest China. J Clim 26:8392–8405
Zhang Q, Li J, Gu X, Shi P (2018) Is the Pearl River basin, China, drying or wetting? Seasonal variations, causes and implications. Global Planet Change 166:48–61
Zhang Y, You Q, Mao G, Chen C, Ye Z (2019) Short-term concurrent drought and heatwave frequency with 1.5 and 2.0 °C global warming in humid subtropical basins: a case study in the Gan River Basin, China. Clim Dyn 52:4621–4641